La mer 51 : 55-72, 2013
Société franco-japonaise d'océanographie, Tokyo

The hydrographic structure along the 137° E line in the western North Pacific from 1990 to 2007

Lamona I. BERNAWIS[1,2], Masao NEMOTO[1] and Jiro YOSHIDA[1]

Abstract : We examined detailed hydrographic structures data along 137°E from 3°N to 34°N from 1990 to 2007 by using CTD. The general oceanic features found along this line agreed well with the results of previous studies using Nansen bottle data. We investigated the activity of double diffusive convection through the histogram plots of the density ratio (R_ρ) and the Turner angle (Tu) to detect the modification processes of water masses in more detail. The region where the stratification is favourable for the onset of salt finger convection ($R_\rho > 3.7$ and $45° < Tu < 60°$) is found just below the bottom half of North Pacific Equatorial Water (NPEW) and North Pacific Tropical Water (NPTW) extending to the upper half of North Pacific Intermediate Water (NPIW). This region existed isopycnally on the surface between 24.0 σ_θ and 26.8 σ_θ persistently along 137°E line. The mode value of R_ρ is 3.48, meaning that the activity of salt finger convection was not so high.

Keywords : *JMA 137° E section, CTD, NPIW core, double diffusive convection, salt finger.*

1. Introduction

The western Pacific Ocean is a region which dominates the dynamics of the climate system in the world. For example, the equatorial processes releasing heat by rain drives the so-called Walker Circulation, and then the equatorial currents redistribute heat. The inter-annual variability of currents and temperatures in the equatorial Pacific modulates the oceanic forcing to the atmosphere; El Niño, for example causes the biggest changes in the equatorial dynamics. In the mid- and high latitude regions, the subtropical and the subarctic gyres redistribute heat from the low latitude to moderate the weather system there (STEWART, 2005).

The current system in the western equatorial Pacific consists of at least four major currents: (1) the North Equatorial Current (NEC) flowing westward between about 20° and 8°N which corresponds to the southern rim of the subtropical gyre, (2) the South Equatorial Current (SEC) flowing westward from about 3°N to 10°S, (3) the narrower North Equatorial Counter Current (NECC) flowing eastward between them, and (4) the Equatorial Under Current (EUC) flowing eastward below the surface straddling the equator over 2°N～2°S. In the region between 20 and 26°N, there is an eastward flowing current known as the Subtropical Counter Current (STCC). The NEC bifurcates into the northward flowing Kuroshio and the southward flowing Mindanao Current. The Kuroshio flows along the Japanese coast, and changes its direction to east off the Joban and Sanriku coast of Japan to form the Kuroshio Extension (KE). The westward counter current known as the Kuroshio Counter Current (KCC) flows between 25 and 30°N. The KE continues to flow eastward as the North Pacific Current (NPC, the northern rim of the subtropical gyre). To the north of subtropical gyre, the subarctic gyre is formed having the

1) Department of Ocean Sciences, Tokyo University of Marine Science and Technology, 4－5－7 Konan, Minato-ku, Tokyo 108－8477, Japan
2) Bandung Institute of Technology, Gedung Labtek XI lt.1, Jl. Ganesha 10, Bandung 40132, Jawa Barat-Indonesia
Jiro YOSHIDA. E-mail: jiroy@kaiyodai.ac.jp

Oyashio as another western boundary current flowing from the eastern coast of Hokkaido to south.

Some major water masses exist in the western Pacific. The North Pacific Intermediate Water (NPIW) is a low salinity water (33.80～34.10) characterized as a vertical salinity minimum around the mid depth (300 m～800 m) originated from the subpolar region (e.g., SVERDRUP *et al.*,1942) extending from 130°E～130°W and 10°N～45°N. Talley (1993) suggested that the Oyashio Winter Water is the source of NPIW, and in the mixed water region between the Kuroshio Extension and the Oyashio front it is modified through some mixing processes to acquire the characteristics of NPIW. This water intrudes into the subtropical gyre as a cross gyre flow and spreads into the mid-depth of the western North Pacific. REID (1965) pointed out that the salinity minimum could be traced on a 26.8 σ_θ surface. The Subtropical Mode Water (STMW) is a minimum of potential density gradient in the 100－400 db layer extending from 130～180°E and 20°N－40°N (MASUZAWA, 1969). The North Pacific Tropical Water (NPTW) is a subsurface salinity maximum (>35.0) water on a 24.0 σ_θ surface caused by excess evaporation over precipitation and by long residence of the surface water in the central Pacific in the 100－200 db layer extending from 130～180°E and 10～25°N (TSUCHIYA *et al.*, 1989). The North Pacific Central Water (NPCW) is a thermocline layer between the NPTW and the NPIW extending from 35°N to 15°N (e.g., SVERDRUP *et al.*, 1942). The North Pacific Equatorial Water (NPEW) is a subsurface salinity maximum (>35.4) at a depth of 150 db from the equator to the south of NPTW covering the whole equatorial Pacific Ocean (e.g., SVERDRUP *et al.*, 1942). The variability and modification of these water masses have been attractive subjects in this area.

Since 1967, the Japan Meteorological Agency (JMA) has been carrying out winter oceanographic surveys along the 137°E from the southern coast of Japan to the area off the New Guinea coast using the R/V Ryofu Maru and Keifu Maru. From 1972, summer observations have begun. Some studies have been conducted using this section to detect the variability of current systems and major water masses cited above (e.g., MASUZAWA, 1969; SUGA *et al.*, 1989; QIU and JOYCE, 1992; Suga and Hanawa, 1995; SHUTO, 1996; BINGHAM *et al,*. 2002).

QIU and JOYCE (1992) extensively analysed the hydrographic features along 137°E observed from 1967 to 1988. Their main purpose was to identify the inter-annual fluctuations in the Kuroshio and KCC, and to understand their relation to the change of the path of the Kuroshio. They also discussed the inter-annual fluctuation in the low latitudes: fluctuation in the transport of NEC and NECC, the surface dynamic height anomalies and the upper mixed layer thickness associated with the ENSO events. Using an analytical model, they found that the inter-annual fluctuations of NEC and NECC were highly correlated with the Sverdrup transport fluctuations. They also discussed the variability of water masses cited above.

SHUTO (1996) used this section to analyse the inter-annual variability of temperature and salinity to discuss the relationship between these variations and the wind forcing. He showed that the temperature changes occurred in the equatorial region of the western North Pacific accompanied by El Niño and La-Niña events, which reached about 20°N where the inclination of isotherms across the NEC fluctuates there. The Empirical Orthogonal Function (EOF) analysis of the winter water temperature resulted in the interruption El Niño and La-Niña events as the first mode, and the decadal changes in SST in the North Pacific as the second mode.

The classical hydrographic observation had been conducted using reversing thermometers and Nansen casts, therefore, QIU and JOYCE (1992) and SHUTO (1996) were obliged to apply the cubic spline fit to vertical discrete data to obtain smooth profiles. Consequently, there were inherent difficulties in detailed analysis such as a variability of the modification process of water masses. This point has been improved by the introduction of CTD observation from 1988. CTD observation becomes as a routine base from 1990. Therefore, taking the advantage of successive CTD data, we try to make detailed water mass analysis using a density

ratio R_ρ (Turner angle: Tu) to grasp the modification processes of major water masses in the present study.

The density ratio or the Turner angle is an indicator of the activity of double diffusive convection (RUDDICK, 1983). The double diffusive convection has two forms; one is the salt finger convection that occurs when a layer of warm and salty water overlies on a layer of relatively cool and fresh water. Another is the diffusive oscillatory convection that occurs when a layer of cool and fresh water overlies on a layer of relatively warm and salty water. For both convections, a fluid layer is statically stable; however, due to the faster diffusion of heat than that of salt give rise to the onset of convection. In both cases, the lower layer becomes dense (up-gradient of density stratification) irrespective of the basic stable stratification. Then, the double diffusive convection should have a certain role in the modification of water masses.

From this point of view, FIGUEROA (1996) and YOU (2002) have investigated the distributions of the density ratio in the world ocean. They showed that double diffusive convection is not so active in the North Pacific ($R_\rho \approx 3 \sim 4$) except at some places where the water masses having distinct contrasts in properties directly contact. The region off Joban-Kashima and Sanriku coast is such a place where the warm/salty Kuroshio and relatively cold/fresh Oyashio waters directly contact each other forming many temperature inversion layers and interleaving structures. Then, these regions are favourable for the onset of double diffusive convection. TALLEY and YUN (2001) and INOUE *et al.* (2003) focused their attention to this point and investigated the role of double diffusive convection on the modification process of NPIW. They both showed that cabbeling and double diffusive convection could explain the total increment of density of NPIW while it extends from the subarctic region to the Sanriku coast. As was mentioned above, various water masses exist along 137°E, and the double diffusive convection should occur in the area sandwiched with the NPTW and NPIW and that below the NPEW. Therefore, in the present paper, focusing on the activity of double diffusive convection along 137°E, we will examine the role of these phenomena on the variability and modification of water masses along 137°E. We describe data analysis process in section 2, followed by hydrographic structures along 137°E from 1990 to 2007 in section 3. We show the characteristics of annual mean and seasonal structures and those associated with ENSO occasionally referring to the previous studies cited above. In section 4, histogram analysis of the density ratio (the Turner angle) is presented to investigate the activity of double diffusive convection. In section 5, we will summarize the results.

2. Data Analysis

We use 35 CTD data from summer and winter cruises (1990－2007) in this study. Basic data by CTD on temperature and salinity at 1 db interval are distributed in ASCII format through CD. Temperature data are converted into potential temperature (θ) and then, potential density is calculated. Stations are located from 34 to 3°N with 1° interval in latitude, except for 40' in the Kuroshio region between 34－32°N. We will use this basic data set for detecting the variability of hydrographic structures. We also use two types of data set: seasonal average data sets at each station and at each depth. The ENSO event average data set in which averaging was made for El Niño, La Niña and Normal periods according to the JMA's criterion of categorizing ENSO event. Since 2006, the JMA has changed the standard for the definition of ENSO event in a certain year from that based on the deviation from 30 years average of 1961～1990 to that of 30 years starting from the year before. Based on this, detailed ENSO events are as follows: El Niño: April 1991 – July 1992, April 1997 – May 1998, June 2002 – February 2003: La Niña: Jul 1995 – February 1996, August 1998 – April 2000, October 2005 – March 2006, February 2007 – March 2008. The other periods are categorized as "Normal". Following QIU and JOYCE (1992), we divide the observational stations into seven bins (Area A – Area G) at an 5° interval (Fig.1).

Following Ruddick (1983), the density ratio and the Turner angle are defined：

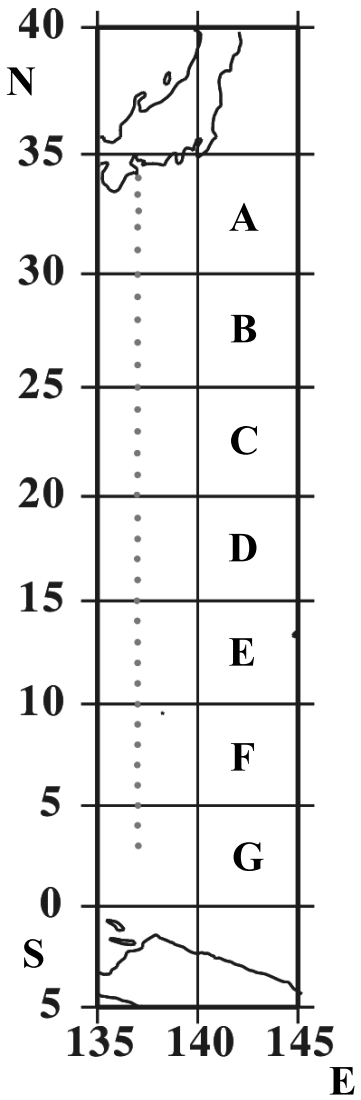

Fig. 1. CTD observation stations along 137°E. Seven areas from A－G are shown.

Density ratio $R_\rho = \frac{\alpha \overline{\theta_z}}{\beta \overline{S_z}}$, where $\alpha = \frac{1}{\rho}\frac{\partial \rho}{\partial \theta}$ and $\beta = \frac{1}{\rho}\frac{\partial \rho}{\partial S}$;

Turner angel $Tu = \tan^{-1}\left(\frac{R_\rho + 1}{R_\rho - 1}\right)$,

where $\overline{\theta_z}$ and $\overline{S_z}$ are mean vertical gradients of potential temperature and salinity, respectively. α and β are the thermal expansion and haline contraction coefficients, respectively. The least square fit over 11 db data is adapted to obtain the mean temperature and salinity gradients. Note that the density ratio is defined as a ratio of temperature gradient on density divided by that of a salinity gradient. When R_ρ is larger than 1 (Tu ranges between 45 and 90°), the salt finger convection occurs, and when R_ρ ranged between 1 and 0 (Tu ranges between －45 and －90°), the diffusive convection occurs. The activity of both convection is intensified as R_ρ becomes unity. Especially, when R_ρ ranged between 1 and 2 (Tu ranges between 72° and 90°), the salt finger convection is so active that salt and heat are efficiently transported downwards and when R_ρ ranges between 0.5 and 1 (Tu ranges between －72 and －90°), diffusive convection is active to transport heat and salt effectively upward. In the present study, Tu is calculated down to 1000 db, because in the Pacific Ocean, the layer below 1000 db is usually statically stably stratified. Histogram plots of Turner angle is presented to know the activity of double diffusive convection. Tu is divided at one degree interval from －90° to 90°, and the number of Tu which falls into each one degree bin is counted, and is divided by the total data number to obtain the occurrence frequency. In this process no averaging was made at each station and at each depth.

3. Hydrographic structures along the 137° E section

3.1 Mean structures of currents and water masses

The basic hydrographic structures seen from the mean of summer/winter cruises are similar to those obtained by QIU and JOYCE (1992). The upheaval of thermocline at 8°N indicates the upwelling region that forms a boundary between the NEC and the NECC (Fig. 2 (a)). The 28°C isotherm at the surface layer marks one of the characteristics features of the western equatorial Pacific Ocean so-called warm pool. The variability of this warm pool is related to the ENSO event. Upward inclinations of isotherms toward north from the surface layer down to a depth of 300 db from 17°N to 25°N indicate the STCC. The thermocline rises sharply

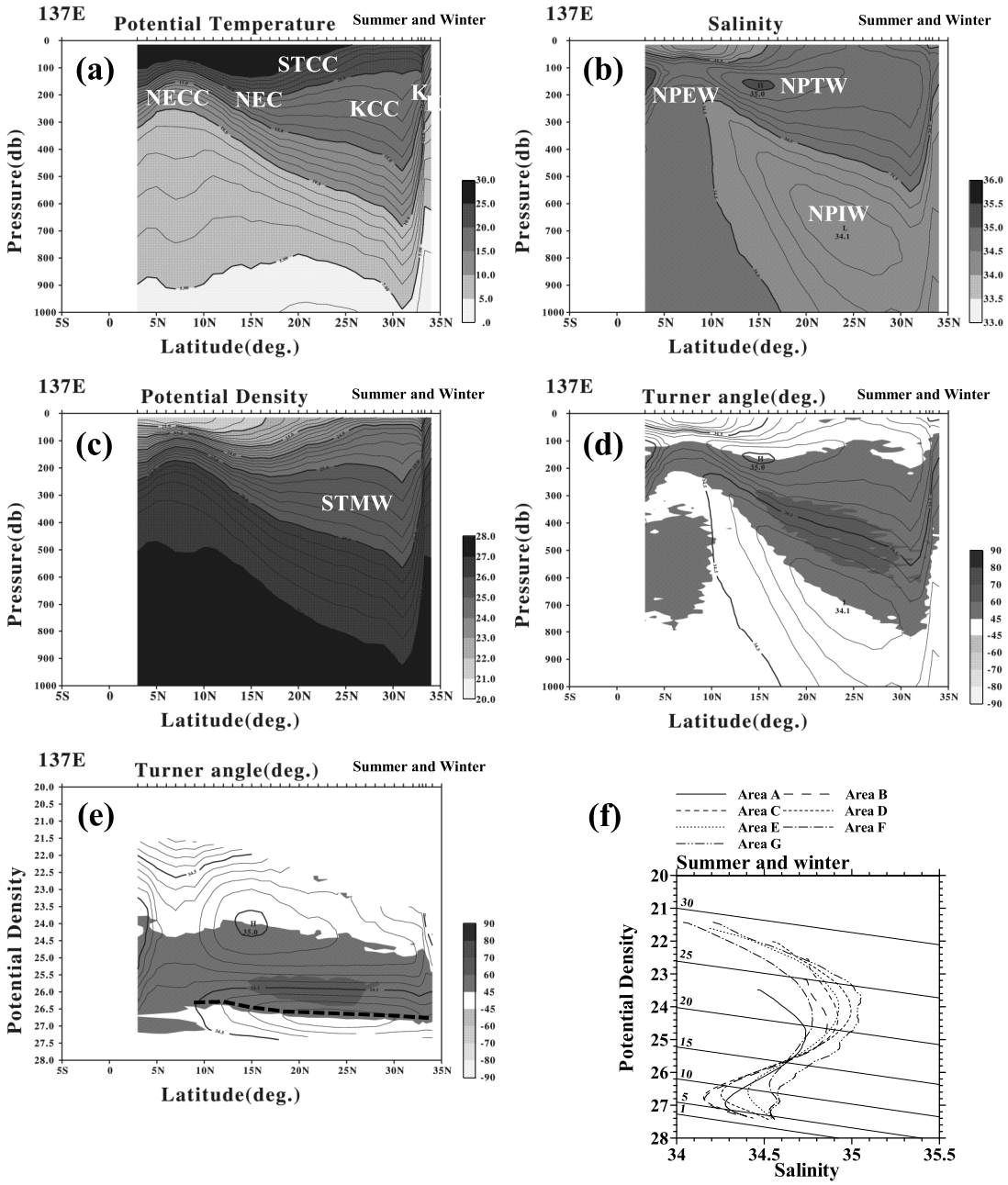

Fig. 2. Vertical cross sections in summer/winter average: (a) potential temperature (interval : 1°C), (b) salinity (interval : 0.1), (c) potential density (interval : 0.1 σ_θ), (d) Turner angle (interval: 10 degree) overlaid on salinity distribution, (e) Turner angle (interval: 10 degree) overlaid on salinity distribution taking σ_θ for the vertical axis and (f) potential density-salinity relation in each area. Solid curves in this figure show potential temperature Dashed line in Fig.2 (e) indicates the extension of salinity minimum. K : Kuroshio, KCC : Kuroshio Counter Current, STCC : Sub-Tropical Counter Current, NEC : North Equatorial Current, NECC: North Equatorial Counter Current, NPIW : North Pacific Intermediate Water, NPTW : North Pacific Tropical Water, NPEW : North Pacific Equatorail Water, STMW : Sub-Tropical Mode Water.

from about 31°N to the Japanese coast, indicating the location of Kuroshio (here, abbreviated as K). The KCC flows westward between 27° N and 31°N.

Two shallow salinity maximums having distinct cores exist near the equator at 150 db and at around 15°N at 160 db (Fig. 2 (b)), respectively. The former corresponds to the NPEW with a salinity exceeding 35.09, and the latter to the NPTW with a salinity exceeding 35.02. The NPEW extends from 3°N to 5°N and its vertical extension is from 80 db to 250 db. QIU and JOYCE (1992) showed that the maximum salinity of the core of NPEW exceeds 35.4 and its location extends from the equator to 5°N. This means that only the northern fraction of NPEW is observed in Fig. 2 (b). In contrast to this limiting extension of NPEW, the NPTW extends broadly from 9°N to 25°N, and its core exist between 13°10′N and 16°40′N. The vertical extension of NPTW is from the surface (at about 25°N) to 300 db (at about 31°N). These two cores of salinity maximums are found roughly at the same isopycnal surface (24.0 σ_θ, Fig. 2 (e)); however, the NPEW exists on rather broad isopycnal layers between 22.6 and 25.9 σ_θ, and the NPTW between 22.6 and 25.3 σ_θ.

In the region from 20 to 30°N and between the depths of 160 and 400 db, the gradient of potential density is weak (Fig. 2 (c)). This water mass is the STMW. SUGA *et al.* (1989) pointed out that a major part of the STMW appearing in this section is formed in the previous winter, and is advected through the KCC.

We can see a broad extension of salinity minimum region from 30°N at a depth of 850 db steeply ascending towards 9°N to a depth of 200 db (Fig. 2 (b)). This salinity minimum water is the NPIW. The core of NPIW (salinity<34.14) lies almost on the 26.8 σ_θ isopycnal surface indicating the extension of the NPIW is essentially an isopycnal process (Fig. 2 (e)): however, it should be noted that the density of salinity minimum become decreased to the south of 15°N.

The region where the stratification is favourable for the onset of salt finger convection (R_ρ> 3.7 and 45°<*Tu*<60°) is found in the bottom half of NPEW and NPTW (Fig. 2 (d)). This region extends to the upper half of the NPIW connecting to the bottom half of the NPEW. Below the NPEW, this region is seen at depths between 400 and 700 db from 3°N to 10°N. The region where relatively active salt finger convection can exist (3.7>R_ρ> 2.7 and 60°<*Tu*<70°) is found just above the core of NPIW between 15 and 30°N. This area is essentially found on isopycnal layers between 25.5 σ_θ and 26.2 σ_θ (Fig. 2 (e)).

A mean potential density-salinity curve was determined for each area (Fig. 2 (f)). A subsurface salinity maximum exists at all areas. It is lowest at Area A (34～30°N) with highest value of density (*S*～34.73, σ_θ～24.78) and becomes more saltier, but less dense towards south (*S*～35.00, σ_θ～24.14) at Area D (20～15°N, NPTW). It becomes less salty at Area E (*S*～34.92, σ_θ～24.00, NPTW) to Area F (*S*～34.77, σ_θ～24.35). At Area G, the subsurface salinity maximum (NPEW) is highest (～35.05) and σ_θ is lowest (～23.66 σ_θ). A salinity minimum (*S*～34.15) corresponding to the core of NPIW is found on 26.8 σ_θ surface at Area B and C (30～20°N). This salinity minimum becomes saltier and less dense towards Area D (*S*～34.25 and ～26.67 σ_θ) and Area E (*S*～34.40 and ～26.58 σ_θ). This feature is also seen in Fig. 2 (e) as a slight upward inclination of a trace of salinity minimum (a dashed line) towards south. This means that the core of NPIW gradually increases its salinity and temperature transported downward in the course of spreading to the south, suggesting the salt finger convection might have a role in this modification process. These values are summarized in Table 1 together with those for summer and winter averages. At Areas F and G, weak salinity maximums (*S*～34.59) are found at 26.88 σ_θ and salinity minimums (*S*～34.52) at 27.2 σ_θ surface. In a layer sandwiched by these minimums and maximums, favorable condition for the onset of salt finger convection is satisfied (Fig. 2 (d)).

3.2 Seasonal structures of currents and water masses

The appearances of currents seen in summer average and winter average (Fig. 3) are essentially same as those in summer/winter

Table 1. Changes in the salinity maximum (S_{max}), salinity minimums (S_{min}) and potential density (σ_θ) from Area A through Area G.

Summer and winter

			NPTW	NPTW	NPTW		NPEW
	Area A	Area B	Area C	Area D	Area E	Area F	Area G
S_{max}	34.73	34.86	34.92	35.00	34.92	34.77	35.05
σ_θ	24.78	24.47	24.35	24.14	24.00	24.35	23.66
	NPIW	NPIW	NPIW	NPIW	NPIW		
S_{min}	34.27	34.15	34.15	34.25	34.40	34.53	-------
σ_θ	26.94	26.80	26.75	26.67	26.58	26.34	-------

Summer

			NPTW	NPTW	NPTW		NPEW
	Area A	Area B	Area C	Area D	Area E	Area F	Area G
S_{max}	34.74	34.87	34.93	34.99	34.94	34.81	35.08
σ_θ	24.97	24.51	24.34	24.10	24.06	24.12	24.43
	NPIW	NPIW	NPIW	NPIW	NPIW		
S_{min}	34.28	34.16	34.15	34.25	34.40	34.53	-------
σ_θ	26.93	26.80	26.76	26.72	26.57	26.39	-------

Winte

			NPTW	NPTW	NPTW		NPEW
	Area A	Area B	Area C	Area D	Area E	Area F	Area G
S_{max}	-------	-------	34.91	35.00	34.94	34.75	35.08
σ_θ	-------	-------	24.33	24.16	24.08	24.36	23.91
	NPIW	NPIW	NPIW	NPIW	NPIW		
S_{min}	34.27	34.15	34.15	34.25	34.39	34.53	-------
σ_θ	26.93	26.81	26.78	26.68	26.59	26.38	-------

averages (Fig. 2); however, the STCC seems to be weakened in winter because the development of mixed layer seems to suppress the upheaval of the isotherms (isopycnals, Fig.3 (c) and (d)). Recently, NOH *et al.* (2007) used eddy-resolving OGCM to reproduce the inter-annual variability of STCC. They showed that the eddy kinetic energy (EKE) in general is highest in summer and lowest in fall, but the value of EKE showed a variation with latitude. Near 19°N, the EKE is highest in summer and lowest in winter that is coincided with our results qualitatively.

Mean structures of water masses in summer is also essentially same as those in summer/-winter averages, except that a high temperature water exceeding 25°C extends farther north to the Kuroshio region (Fig. 3 (a)). In winter, as was mentioned above, the surface mixed layer develops to a depth of 180 db at 31°N and gradually shallows toward south (Fig. 3 (b)). As a consequences of the deepening

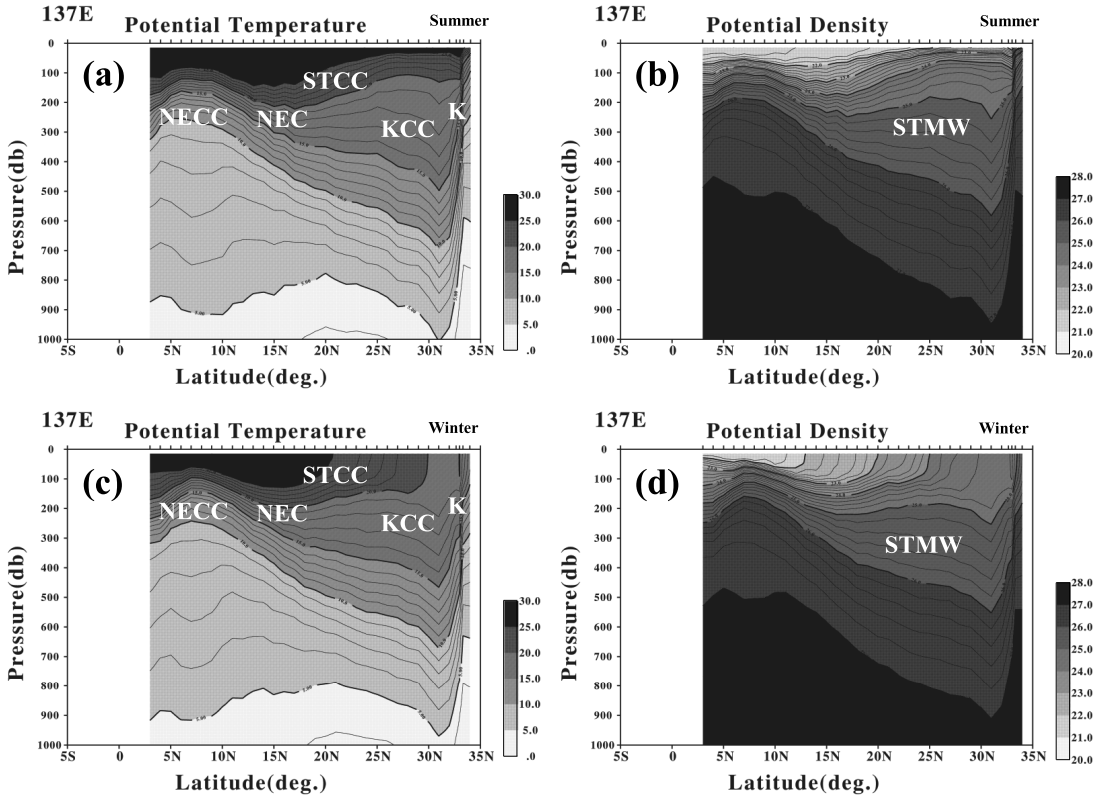

Fig. 3. Vertical cross sections of (a) potential temperature and (b) potential density in summer, and (c) potential temperature and (d) potential density in winter. Abbreviations in the figure are as same as in Fig. 2.

of the mixed layer, the gradient of potential density in the STMW area becomes large (for example, the upheaval of 25.0 σ_θ is suppressed around 25°N at a depth of 200 db), suggesting the weakening of the STMW in winter (Fig. 3 (d)). The salinities at the cores of NPTW, NPEW and NPIW do not change seasonally; however, σ_θ at these cores slightly changed especially for the salinity maximums of NPTW and NPEW (Table 1). The slight upward inclination of salinity minimum of NPIW is also seen in summer and winter, respectively (not shown here).

3.3 ENSO composite structures of currents and water masses

In the summer of El-Niño periods (1991, 1992, 1998, 2002), upheaval of isotherms intensified in the surface layer between 30 and 25°N forming a distinct boundary between the KCC and the STCC (Fig. 4 (a)), suggesting these currents become strong during the El-Niño summer. QIU and JOYCE (1992) calculated the geostrophic transport of KCC, and showed that the KCC has a tendency of increasing its transport in summer, but strongly affected by the Kuroshio path, namely, in a meandering year, the KCC reduces its transport. However, they did not show any tendency of variability of geostrophic transport of KCC among El-Niño, La-Niña and Normal periods. Thermal structure in La-Niña and Normal summer is almost identical (Fig. 4 (c) and 4 (e)). In the winter of El-Niño periods, the area of high temperature layer (>25°C) does not reach beyond 20°N as is so for La-Niña and Normal periods (Figs. 4 (b), 4 (d) and 4 (f)).

Salinity distributions show changes in the

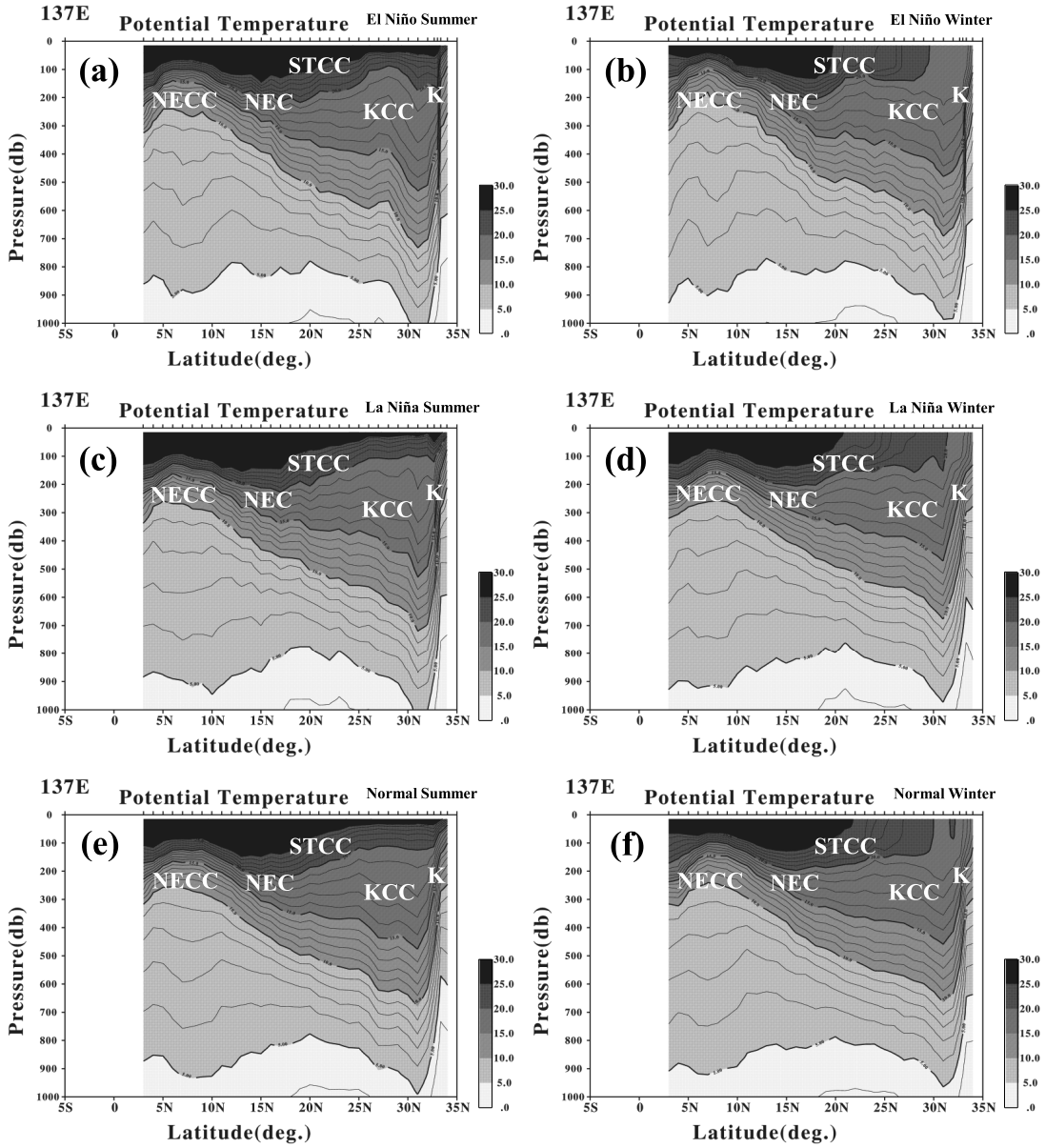

Fig. 4. Vertical cross sections of potential temperature in (a) El Niño summer and (b) El Niño winter, (c) La Niña summer, and (d) La Niña winter, (e) Normal summer and (f) Normal winter. Abbreviations in the figure are as same as in Fig. 2.

surface layer above 300 db during ENSO periods. A low salinity water (<34.00) appears at the surface between 3 and 11°N in La-Niña summer and between 7 and 11°N in La-Niña winter suggesting the excess precipitation in the equatorial area during La-Niña periods (Fig. 5 (c) and (d)). In El-Niño periods, low salinity water patches appeared at a depth of 200 db (Figs. 5 (a) and (b)) near 5°N. This water is found at almost same density surface to that of NPIW centered on 26.5 σ_θ isopycnal surface (Figs. 6 (a) and (b)). The formation or

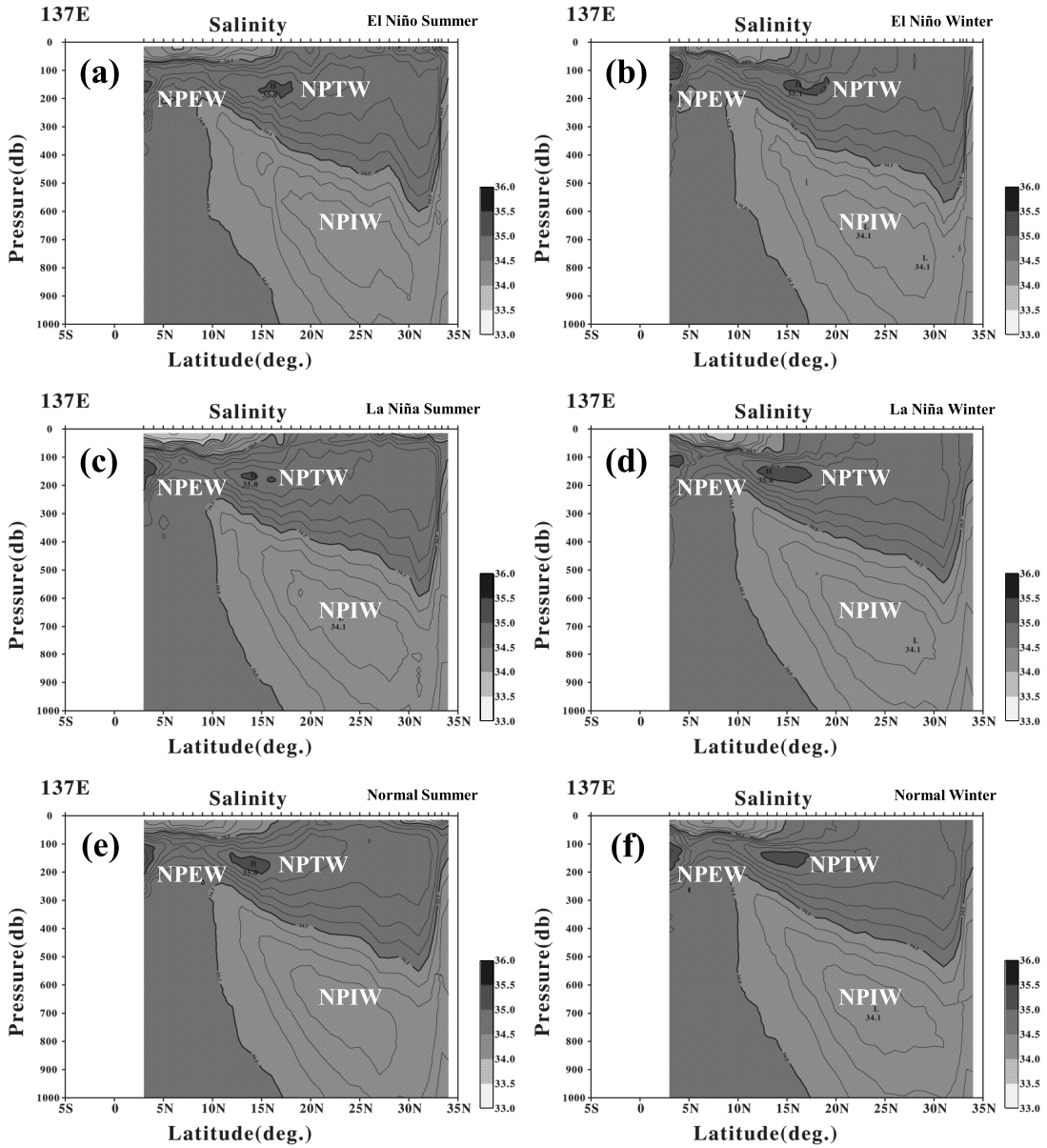

Fig. 5. Same as in Fig. 4, but for salinity.

transportation mechanism of this low salinity water in El-Niño periods is unclear at present. Salinity distributions in Normal summer and winter (Figs. 5 (e) and (f)) are almost identical to those of summer/winter average (Fig. 2 (b)).

Mean potential temperature-salinity curves were determined for each area, and at Area G, distinct ziggy structures are found during El-Niño periods (Fig. 7 (a) and (b)). These structures are also found in La-Niña and Normal periods to the lesser extent (Fig. 7 (c), (d), (e) and (f)), indicating the high variability of equatorial region especially during El-Niño

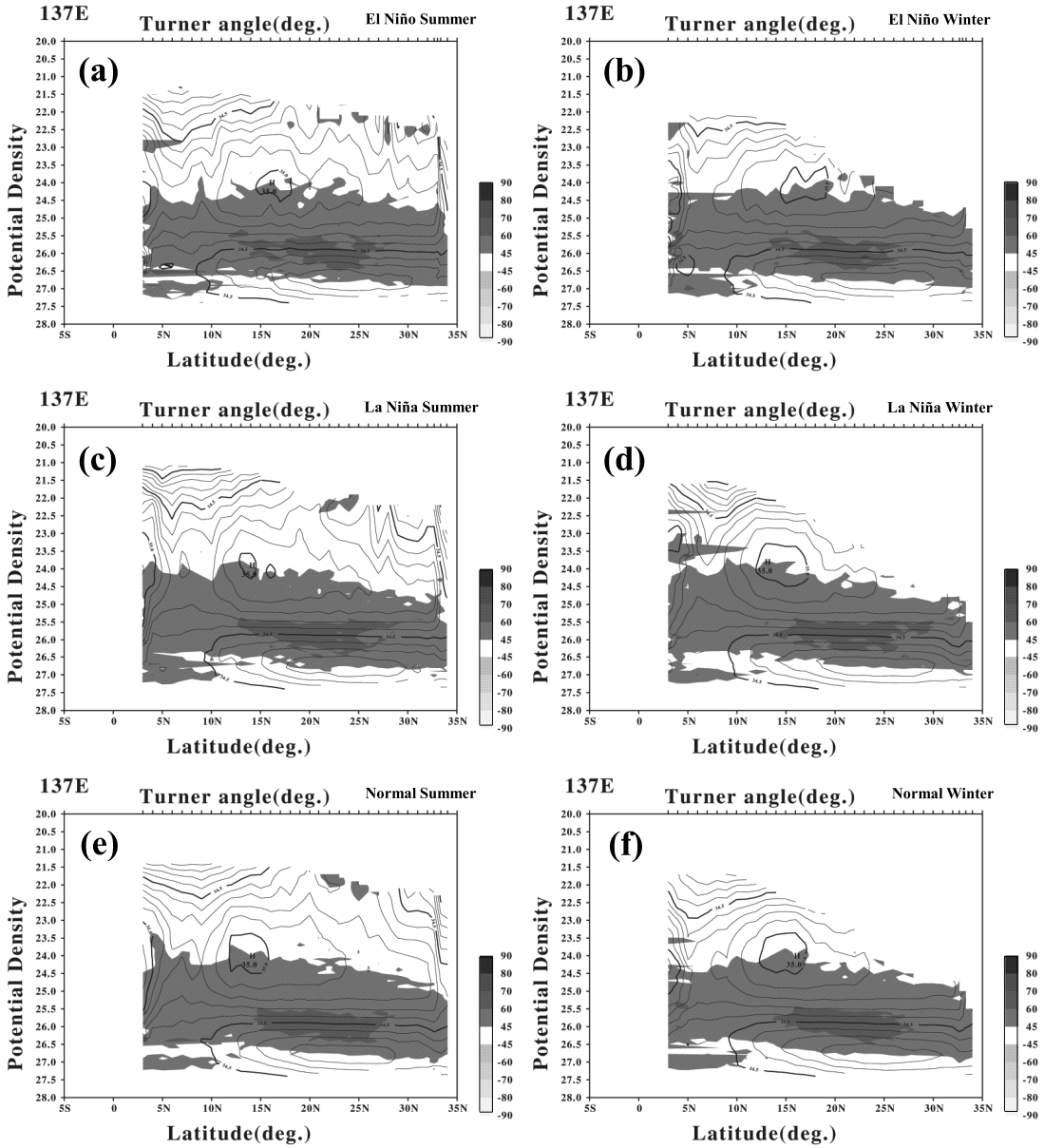

Fig. 6. Same as in Fig. 4, but for Turner angle (interval: 10 degree) overlapped on salinity distribution taking σ_θ for the vertical axis.

periods. These ziggy structures are possibly caused by the intrusion of saline or less saline water from the surrounding area. It is interesting to note that these intrusions essentially exist along isopycnal surfaces without temperature inversions as is often seen in the frontal area where eddies or water masses having distinct contrast in temperature and salinity collide (e.g., HEBERT *et al.*, 1990; YOSHIDA, 2003). RICHARDS and BANKS (2002) showed the existence of such intrusion layers (sometimes called as "interleaving" because of the existence

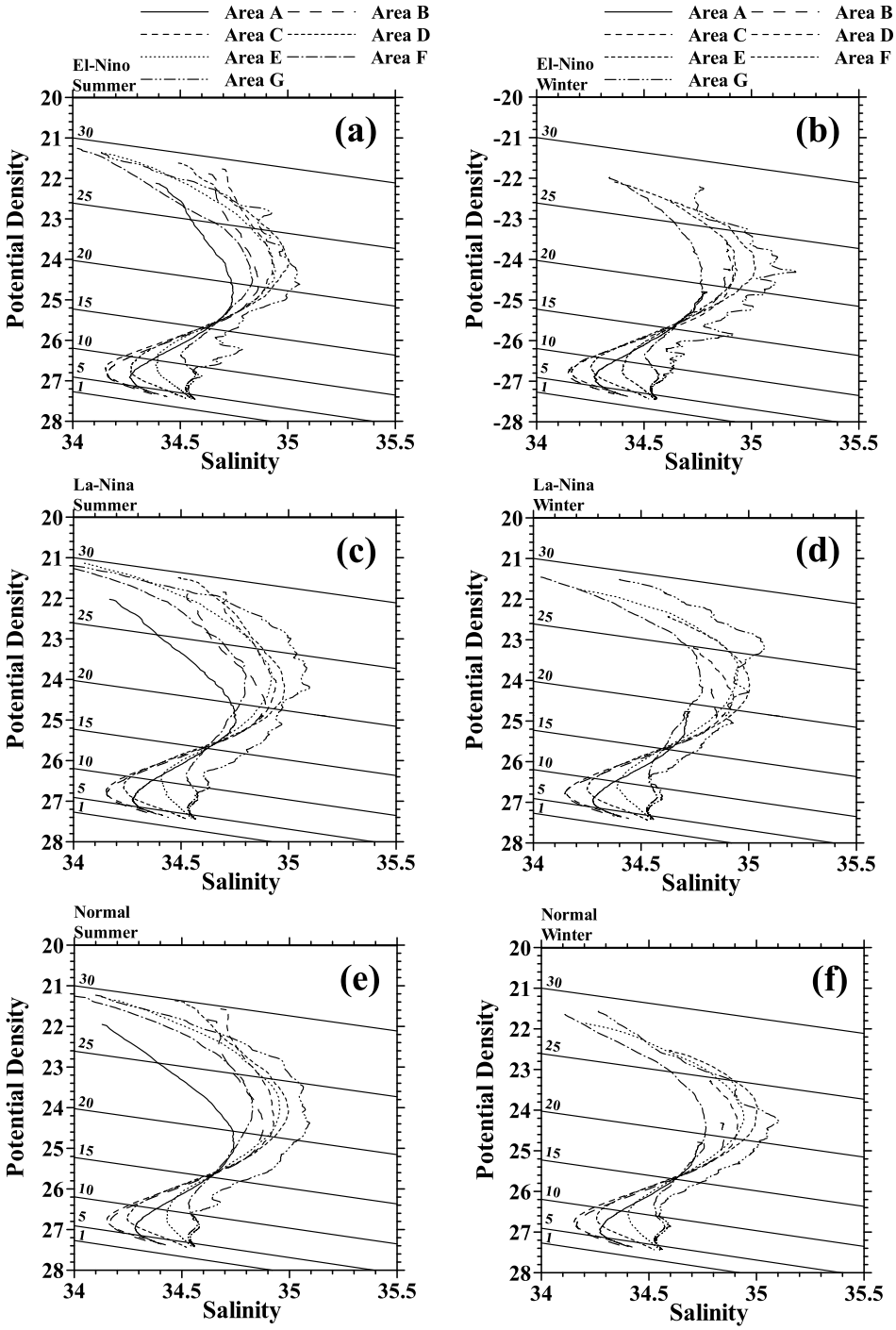

Fig. 7. Potential density-salinity relation in each area for (a) El Niño summer and (b) El Niño winter, (c) La Niña summer and (d) La Niña winter, (e) Normal summer and (f) Normal winter. Solid curves in these figures show the potential temperature.

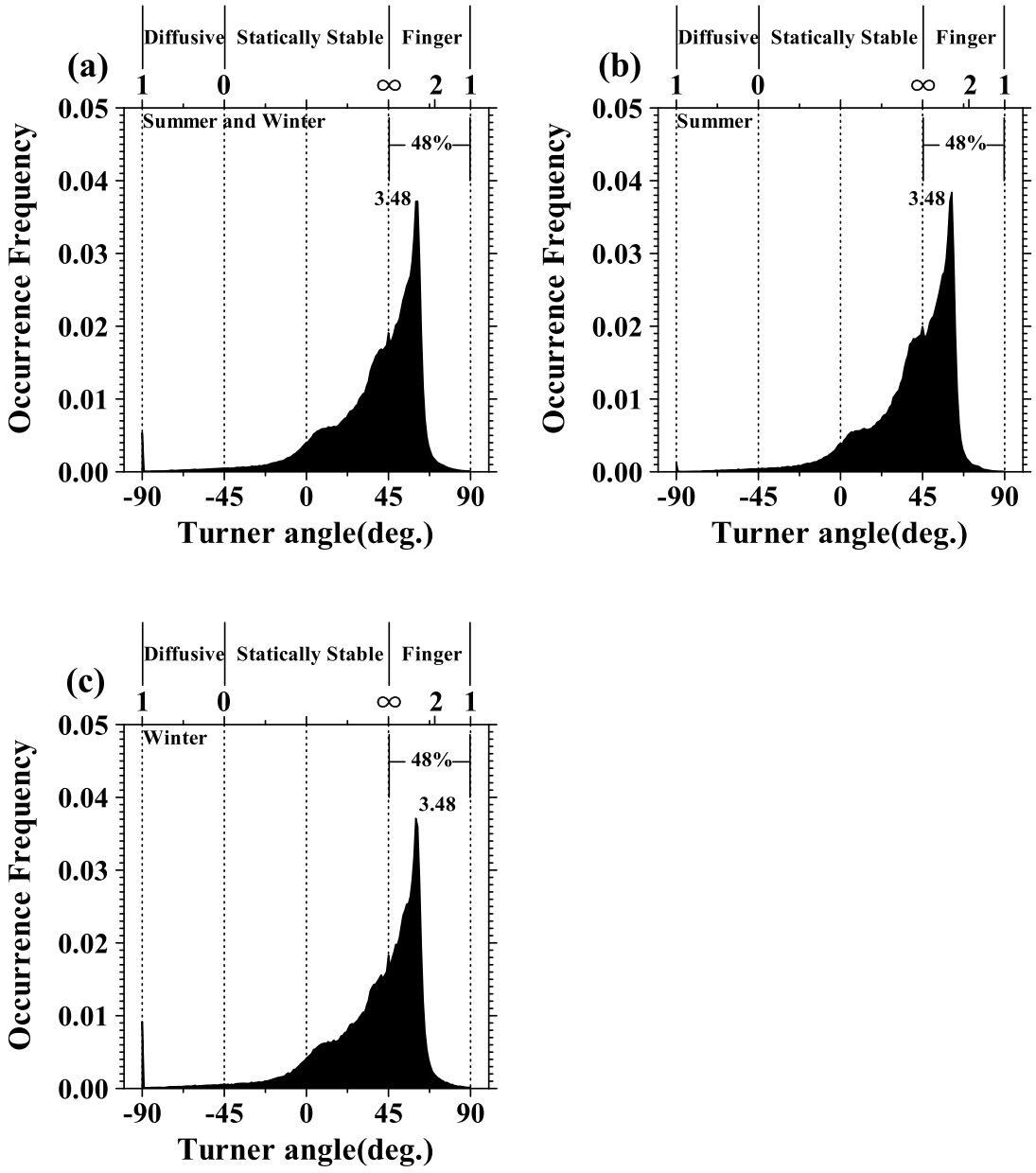

Fig. 8. Histograms of the occurrence frequency of Turner angle for (a) summer/winter, (b) summer, and (c) winter.

of warm/salty and cool/fresh layers piling up alternatively) crossing the equator from 3°S to 3°N along 165°E during La-Niña period and from 5°S to 5°N along 156°E during El-Niño period. They concluded that the observed interleaving is the persistent feature in the equatorial Pacific, and are possibly caused by both double-diffusive instability and inertial instability. The region of salt finger favorable layer does not show remarkable change

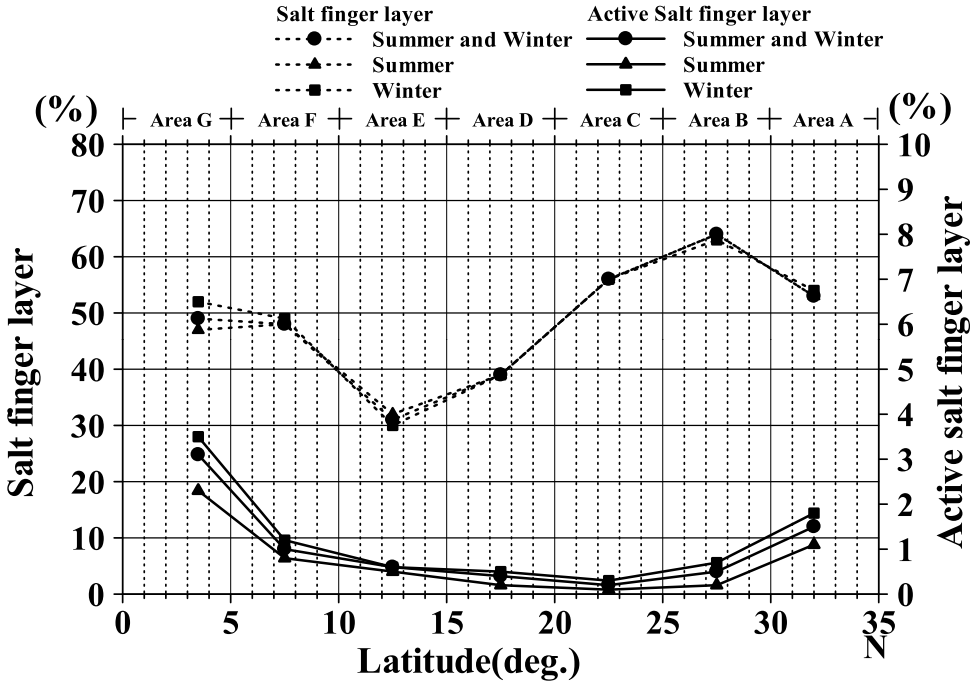

Fig. 9. Latitudinal change of the percentage of salt finger convection (● : summer and winter, ▲ : summer, ■ : winter with dotted lines) and the active salt finger convection (● : summer and winter, ▲ : summer, ■ : winter with solid lines)

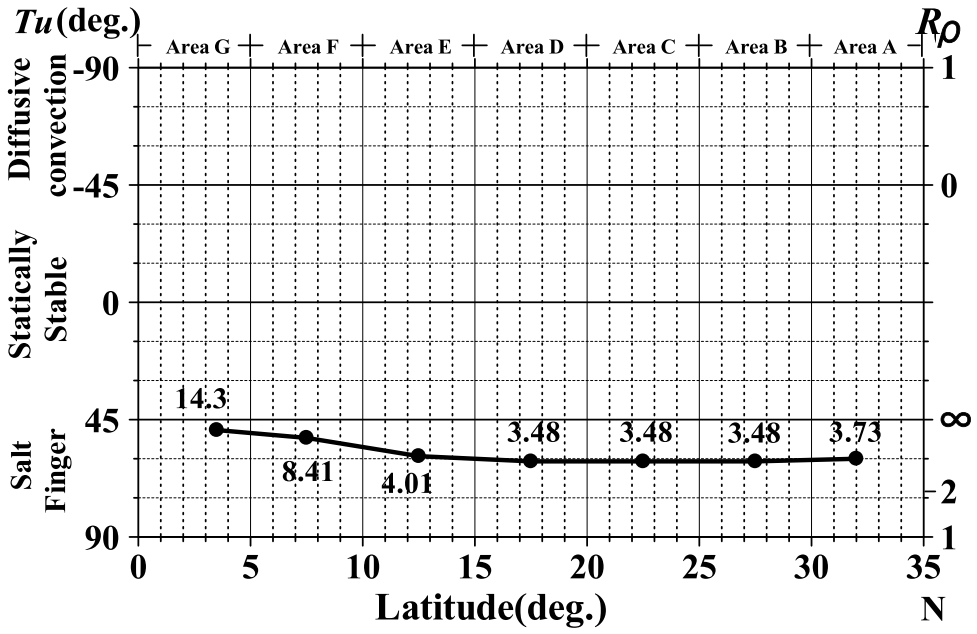

Fig. 10. Latitudinal change of Turner angle (density ratio).

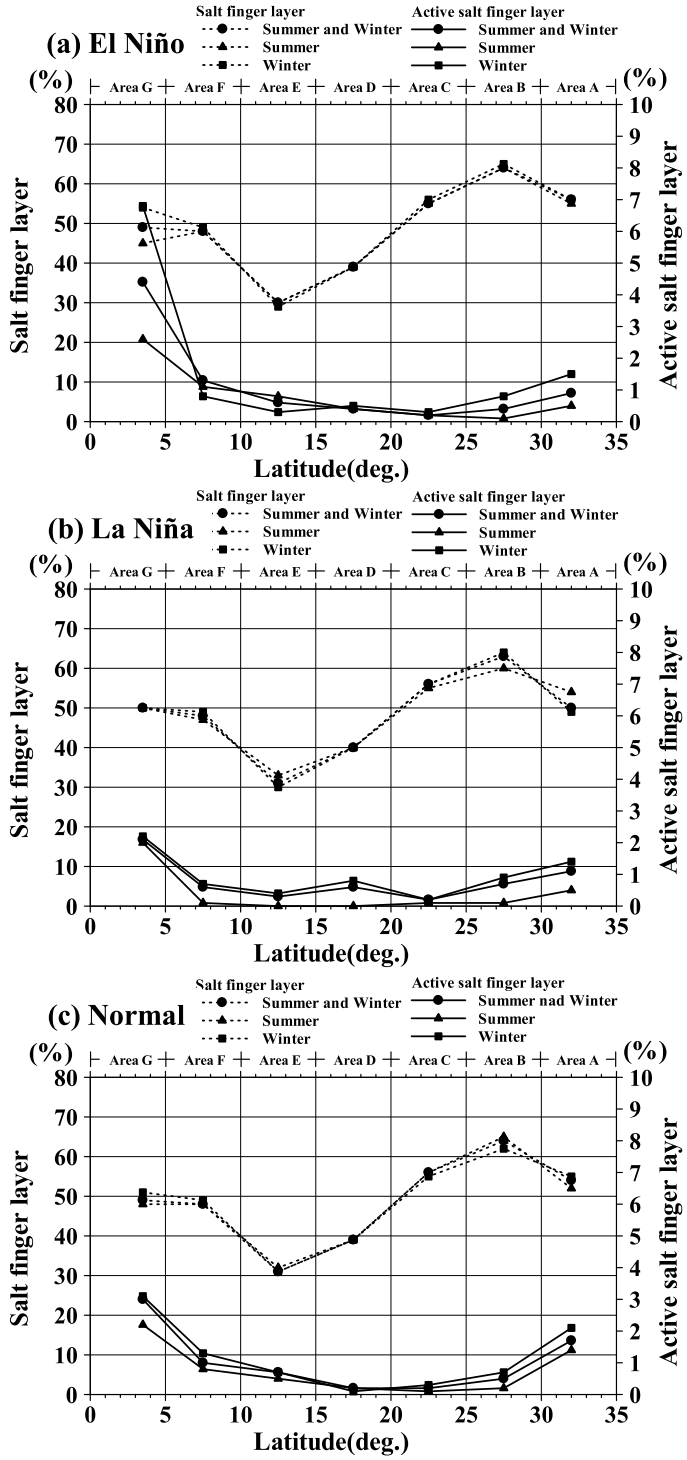

Fig. 11. Same as in Fig. 9, but for (a) El Niño, (b) La Niña and (c) Normal periods.

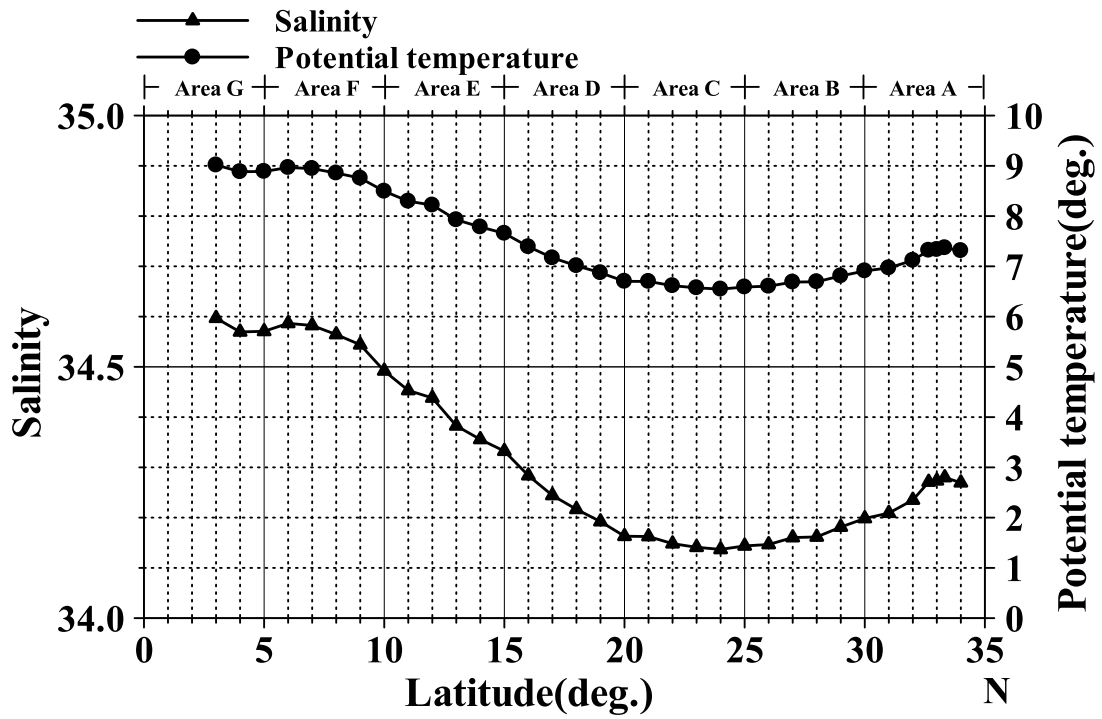

Fig. 12. Latitudinal distribution of salinity (●) and potential temperature (▲) on a 26.8σ_θ surface.

between the ENSO and Normal periods (Fig. 6). This point will be discussed in the following section.

4. Histogram analysis of Turner Angle (*Tu*)

Histogram plots of *Tu* in (a) summer and winter, (b) summer only and (c) winter only show no remarkable seasonal variability (Fig. 8). The salt finger favourable layer occupies 48% in the total layer down to 1000 db. The mode (a peak of occurrence frequency) of *Tu* appears in the salt finger regime, and is 61 degree ($R_\rho \approx 3.48$), meaning that almost half of the stratification is favorable for onset of salt finger convection; however, its activity is not so high along 137°E. This value is within the range those obtained by FIGUEROA (1996) and YOU (2002) in the central Pacific Ocean.

In each area, such histogram plots of *Tu* were conducted to obtain area to area variability of the activity of salt finger convection and summarized in Figs. 9 and 10. The percentage of salt fingering layer in each area does not change seasonally, which was above 50% from Area A thorough Area C (34°N to 20°N), being the highest in Area B (29°N to 25°N), where the core of NPIW just exists. It gradually decreases to Area E (14 to 10°N corresponding to the southern edge of NPIW), and increases to about 50% at Areas F and G (Fig. 9 (a)) because of high salinity in the upper layer in these areas. The mode value of R_ρ in each area also does not change seasonally. It gradually increases towards south (Fig. 10). The high mode values in Area F and Area G mean that the activity of salt finger convection is low in these areas. The active salt finger regime ($72° < Tu < 90°$, $1 < R_\rho < 2$) behaves differently. Namely, the percentage of active salt finger layer is generally small over the entire area, but is relatively high in Areas A, F and G, especially in winter (see Fig. 9). This tendency is distinct during El-Niño winter (Fig. 11). The percentage of active salt finger regime is high and is up to 7%. This higher value should be due to the development of ziggy structures in El-Niño

winter (Fig. 7 (b)). The percentage of salt finger layer and modes of do not change from seasonal average among El-Niño, La-Niña and Normal periods.

5. Summery

In the present study, we investigated in detail the variability of hydrographic structure along 137°E line using CTD data obtained from 1990 through 2007. We compared our results to those obtained by classical Nansen cast data from 1966 through 1989. In addition, we first apply density ratio analysis along 137°E line to discuss the effect of double diffusive convection. Some results are summarized as follows;

(1) The region where the stratification is favourable for the onset of salt finger convection ($R_\rho > 3.7$ and $45^\circ < Tu < 60^\circ$) is found in the bottom half of North Pacific Equatorial Water (NPEW) and North Pacific Tropical Water (NPTW), which extends to the upper half of North Pacific Intermediate Water (NPIW). This region exists isopycnally on the surface between $24.0\,\sigma_\theta$ and $26.8\,\sigma_\theta$ persistently along 137°E line.

(2) A slight upward inclination of a trace of salinity minimum along the NPIW core is detected, suggesting that salt finger convection might play a role in modification of the NPIW.

(3) The percentage of salt finger layer occupying in the total layer down to 1000 db along 137°E line is about 48%. The mode value of Tu is 61 degree ($R_\rho \approx 3.48$). These values do not change seasonally and in ENSO periods; however, it changes regionally, as is relatively high in mid-latitude and equatorial region, and is low in the lower latitude.

(4) The active salt finger convection is anticipated in equatorial region (3°N to 5°N) especially in El-Niño winter. The high activity of salt finger convection might be associated with the development of interleaving structure in this region.

Acknowledgements

This work is a part of Ph.D. thesis of Lamona I. Bernawis at the Tokyo University of Marine Science and Technology. This work was supported by Grant-in-Aid for Scientific Research from the Ministry of Education, Culture, Sports, Science and Technology of Japanese Government are greatly appreciated..

References

BINGHAM, F.M., T. SUGA and K. HANAWA (2002): Origin of waters observed along 137°E. J. Geophys. Res., **107**(C12), 3073, doi : 10.1029/2000JC000722.

FIGUEROA, H. A. (1996): World ocean density ratios. J. Phys. Oceanogr., **26**, 267－275.

HEBERT, D., B.R. RUDDICK and N.S. OAKEY (1990): Evolution of a Mediterranean salt lens: Scalar properties, J. Phys. Oceanogr., **20** (9), 1468－1483.

INOUE, R, J. YOSHIDA, Y. HIROE, K. KOMATSU, K. KAWASAKI and I. YASUDA (2003): Modification of North Pacific Intermediate Water around Mixed Water Region. J. Oceanogr., **59**, 211－224.

MASUZAWA, J. (1969): Subtropical Mode Water. Deep-Sea Res., **16**, 463－472.

NOH, Y., B. Y. YIM, S. H. YOU, J. H. YOON and B. QIU (2007): Seasonal variation of eddy kinetic energy of the North Pacific Subtropical Countercurrent simulated by an eddy-resolving OGCM. Geophys. Res. Lett., **34**, L07601, doi : 10.1029/2006GL029130

QIU, B. and T. M. JOYCE (1992): Interannual variability in the mid- and low-latitude Western North Pacific. J. Phys. Oceanogr., **22**, 1092－1079.

REID, J. L. (1965): Intermediate Waters of the Pacific Ocean. The Johns Hopkins Oceanographic Studies, No. 2, The Johns Hopkins Press, Baltimore, 85 pp.

RICHARDS, K. J. and H. BANKS (2002): Characteristics of interleaving in the western equatorial Pacific, J. Geophys. Res., **107** (C12), 3231, doi : 10.1029/2001JC000971.

RUDDICK, B.R. (1983). A practical indicator of the stability of the water column to double-diffusive activity. Deep-Sea Res., **30**, 1105－1107.

SHUTO, K. (1996): Interannual variations of water temperature and salinity along the 137°E Meridian. J. Oceanogr., **52**, 575－595.

STEWART, R.H. (2005): Introduction to Oceanography. Department of Oceanography. Texas A&M University. 344pp.

SUGA, T. and K. HANAWA (1994): Interannual variations of North Pacific Subtropical Mode Water in the 137°E Section. J. Phys. Oceanogr., **25**, 1012－1017.

SUGA, T., K. HANAWA and Y. TOBA (1989): Subtropical Mode Water in the 137°E section. J. Phys. Oceanogr., **19**, 145－175.

SVERDRUP, H. U., M. W. JOHNSON and R. H. FLEMING (1942): The Oceans: Their Physics, Chemistry and General Biology. Prentice-Hall, Englewood

Cliffs, New York, 1087 pp.
TALLEY, L. D., (1993): Distribution and formation of North Pacific Intermediate Water. J. Phys. Oceanogr., **23**, 517−537.
TALLEY, L. D. and J. Y. YUN (2001): The role of cabbeling and double diffusion in setting the density of the North Pacific Intermediate Water salinity minimum. J. Phys. Oceanogr., **31**, 1538−1549.
TSUCHIYA, M., R. LUKAS, R. A. FINE, E. FIRING and E. LINDSTROM (1989): Source waters of the Pacific Equatorial Undercurrent. Progr. Oceangr., **23** (**2**), 101−147.
YOSHIDA, J. (2003): The activity of double diffusive convection investigated through the density ratio distribution in the Mixed Water Region (MWR) off Joban-Kashima and Sanriku Coasts to the north-east of Honshu, Japan. La mer, **41**, 52−59.
YOU, Y. (2002): A global ocean climatological atlas of the Turner angle: implications for double-diffusion and water-mass structure. Deep-Sea Res., **49**, 2075−2093.

Received: November 2, 2007
Accepted: December 17, 2007
Final form: March 11, 2013